Supplemental Information

Single-Cell Imaging of Metastatic

Potential of Cancer Cells

Krishna Midde, Nina Sun, Cristina Rohena, Linda Joosen, Harsharan Dhillon, and Pradipta Ghosh

TRANSPARENT METHODS:

Reagents and Antibodies: All reagents used in this study are of research grade and obtained from Sigma-Aldrich (St. Louis, MO) unless otherwise specified. Cell culture media were purchased from Invitrogen (Carlsbad, CA). EGF (Invitrogen), Insulin (Novagen), Lysophosphatidic Acid (LPA) (Sigma) and PDGF (Invitrogen) were obtained commercially. The Src inhibitor PP2 was obtained from Calbiochem. Receptor Tyrosine Kinase inhibitors Erlotinib (ChemieTek, Indianapolis, IN. Cat # CT-EL002) and Lapatinib (LC laboratories. Cat # L-4899) drugs were generously donated by Frank Furnari (Ludwig Cancer Institute - UCSD). Docetaxel was commercially obtained from Sigma Aldrich (cat # 01885). Mouse monoclonal antibodies against pTyr (BD Biosciences, cat # 610000), GFP (Santa Cruz Biotechnology), HA (Covance), total (t)ERK (Cell Signaling) and tubulin (Sigma) were purchased from commercial sources. Rabbit polyclonal antibodies against GIV-CT (Girdin T-13, Santa Cruz Biotechnology), phospho-Akt S473 (Cell Signaling), and phospho-ERK 1/2 (Cell Signaling) were obtained commercially. Rabbit monoclonal antibodies against pY1068 EGFR and total (t)Akt were obtained from Cell Signaling and anti-pY1764 GIV antibodies were obtained from Spring Biosciences (Lopez-Sanchez et al., 2014). Anti-mouse and anti-rabbit Alexa-594- and Alexa-488-coupled goat secondary antibodies were used for immunofluorescence. Goat anti-rabbit and goat anti-mouse Alexa Fluor 680 or IRDye 800 F(ab')2 for immunoblotting were from Li-COR Biosciences (Lincoln, NE). Rabbit or mouse IgGs used as negative controls in immunoprecipitation was purchased from BioRad (Hercules, CA) and Sigma (St. Louis, MO), respectively.

Plasmid Constructs: IMP-FRET probes encoding different stretches of GIV's C-terminus encompassing either one or both critical tyrosines, Y1764 and Y1798 of GIV were generated using the cloning strategy previously described for the '*phocus-2nes*' FRET probe that was used to measure functional phosphorylation of the adaptor protein IRS-1 (Sato et al., 2002). Briefly, fragment cDNAs of mutant ECFP (mutations are F64L, S65T, Y66W, N146I, M153T, V163A and N212K), mutant EYFP (mutations are S65G, V68L, Q69K, S72A and T203Y), various stretches of substrate domain from human GIV (Accession# BAE44387; see **Fig S3b**), phosphorylation recognition domain [the N-terminal SH2 domain, residues 330-429 from the p85α subunit of bovine PI3K (Accession# NM_174575), which is reported to bind both critical tyrosines within GIV's C-terminus (Lin et al., 2011)] were generated by standard PCR and cloned into the restriction sites shown in **Fig 1c**. A nuclear-export signal sequence (NES) – LPPLERLTL (Ullman et al., 1997), was inserted to retain the IMP probe in cytosol. Amino acid sequences of flexible linker LnL10 and LnL20 are GNNGGNGGSNNGGNNGNGG and GNNGGNGGSNNGNGGGNGNNGGNNGNGG, respectively. Various IMP constructs, as illustrated in **Fig S3b**, were subcloned between HindIII and XbaI sites of pcDNA 3.1(+) vector (Invitrogen Co., Carlsbad, CA) using Fast Cloning Technique (Li et al., 2011). There are two noteworthy specifics in our chosen paired fluorophores: 1) Q69K mutation in eYFP: Q69 is fairly close to the chromophore anion inside the β-barrel of YFP. It was previously reported that Q69K could promote the anionic form of the chromophore to hinder its protonation, and therefore reduce the apparent pK_a to 6.1, with little effect on its other sensitivities (Griesbeck et al., 2001). 2) The commonly used dimerization preventing mutation (A206K) was not present in our construct. Prior work has carefully documented that this mutation renders probes that require conformational changes to monitor dynamic signaling events non-functional because such conformational changes depend on the weak dimerization, and yet, does not produce significant artifacts of intermolecular dimerization-related FRET (Jost et al., 2008; Kotera et al., 2010). The sequences of primers that were used for cloning IMP constructs are available upon request. GFP-Akt-PH was obtained from R. Tsien (UCSD) and previously used as a reporter to study GIV-dependent activation of PI3K in cells (Lin et al., 2011). C-terminal HA-tagged c-Src for mammalian expression was generated by cloning the entire coding sequence into pcDNA 3.1 between Xho I and Eco RI. HA tagged SHP-1 was used and validated previously (Mittal et al., 2011). All constructs were checked by DNA sequencing prior to their use in various assays.

Cell Lines: MDA-MB-231, PC-9 and H2030 parental and their brain metastatic (BrM) counterparts listed in **Fig. S5b** were generous gifts from Joan Massagué (Memorial Sloan Kettering Cancer Center, New York). Briefly, metastatic cells were isolated from either lymph node or pleural effusions of cancer patients and selected in nude mice to

generate the BrM subclones, which are known to exhibit higher invasiveness and metastatic proclivity to brain and bone (Nguyen et al., 2009; Valiente et al., 2014). The 21T series (16N, NT and MT2) cancer cell lines isolated from different stages of breast cancer progression were generous gifts from Arthur B. Pardee (Dana-Farber Cancer Institute, Harvard Medical School) and cultured as described earlier (Garcia-Marcos et al., 2011; Souter et al., 2010). Hs578T cells were obtained from ATCC, and their Docetaxel-resistant subclones were generated according to the protocol developed by Andrew C. Schofield et al (Brown et al., 2004). Briefly, cells were exposed to incremental concentrations of sub-lethal doses of docetaxel on a daily-basis for 1 hr, followed by splitting and recovery until stable revival of growth in media with drug concentration of 30 µM was achieved. Erlotinib and Lapatinib resistant HCC827 were generous gifts from Frank Furnari (Ludwig Cancer Institute – UCSD). Unless mentioned otherwise, cell lines used in this work were cultured according to ATCC guidelines, or guidelines previously published for each line.

Transfection and Cell Lysis: Transfection was carried out using Genejuice (Novagen) or Mirus LT1 (Mirus) for DNA plasmids as previously described (Garcia-Marcos et al., 2009; Ghosh et al., 2010). Lysates were prepared by resuspending cells in lysis buffer [20 mM HEPES, pH 7.2, 5 mM Mg-acetate, 125 mM K-acetate, 0.4% Triton X-100, 1 mM DTT, supplemented with sodium orthovanadate (500 µM), phosphatase (Sigma) and protease (Roche) inhibitor cocktails], after which they were passed through a 30G needle at 4°C, and cleared (10-14,000 g for 10 min) before being used in subsequent experiments.

In cellulo **phosphorylation assays**: Cos7 cells expressing the indicated IMP probes in various assays were starved overnight at ~30 h after transfection, and subsequently treated with 0.2 mM Na_3VO_4 for 1 h prior to stimulation with growth factors or GPCR ligands. Cells were then washed with chilled PBS at 4°C that was supplemented with 500 µM Na_3VO_4, lysed using ~400 µl of lysis buffer, and equal aliquots of lysates (~1-2 mg of total protein) were incubated for 4 hours at 4°C with either anti-GFP mouse monoclonal antibody (1 µg) (Lane et al., 2008) or control mouse IgG. Protein G Sepharose beads (GE Healthcare) were then added to the lysates and incubated at 4°C for additional 60 min. Beads were then washed 3 times using 1 ml of lysis buffer, and immune complexes were eluted by boiling in Laemmli's sample buffer. For steady state in vivo phosphorylation assays, IMP probes were co-transfected with Src or SHP1 constructs, and after 48 h of transfection cells were lysed and immunoprecipitated with anti-GFP mAb exactly as described for assays using ligand stimulation. In all assays tyrosine phosphorylation of IMP probes was detected by dual color immunoblotting with anti-pTyr mAb (BD Biosciences; Cat # 610000) and rabbit polyclonal anti-GFP using LiCOR Odyssey. Presence of yellow pixels on overlay of pTyr (green) and GFP (red) was interpreted as tyrosine phosphorylation of the IMP probe.

Scratch-wound healing assays: Sub-confluent (~85-90%) monolayers of HeLa cells were transiently transfected (exactly as outlined above) within 6-8 h after splitting with IMP constructs, grown to confluence over 24-30 h prior to scratch-wounding with the tip of a 200 µl pipette. The media was changed immediately afterwards to remove the scraped cells and avoid them from settling down. Wounds were imaged immediately after wounding at designated spots. The exact same coordinate was imaged again after 12 and 24 hours by light microscopy. Images were analyzed using ImageJ by outlining the borders of the wound at the beginning and end of the assay time points.

Förster Resonance Energy Transfer (FRET) studies: Intramolecular FRET was detected by sensitized emission using the three-cube method were performed as previously reported by Midde et al (Midde et al., 2015). All fluorescence microscopy assays were performed on single cells in mesoscopic regime to avoid inhomogeneities from samples as shown previously by Midde et al. (Borejdo et al., 2012; Midde et al., 2014). Briefly, cells were sparsely split into sterile 35 mm MatTek glass bottom dishes and transfected with 1 µg of various IMP constructs illustrated in **Fig. S3b**. An Olympus IX81 FV1000 inverted confocal laser scanning microscope was used for live cell FRET imaging (UCSD-Neuroscience core facility). The microscope is stabilized on a vibration proof platform, caged

in temperature controlled (37°C) and CO_2 (5%) supplemented chamber. A PlanApo 60x 1.40 N.A. oil immersed objective designed to minimize chromatic aberration and enhance resolution for 405-605 nm imaging was used. Olympus Fluoview inbuilt software was used for data acquisition. A 515 nm Argon-ion laser was used to excite EYFP and a 405 nm laser diode was used to excite ECFP as detailed by Claire Brown's group (Broussard et al., 2013). Spectral bleed-through coefficients were determined through FRET-imaging of donor-only and acceptor-only samples (i.e. cells expressing a single donor or acceptor FP). Enhanced CFP emission was collected from 425-500 nm and EYFP emission was collected through 535-600 nm and passed through a 50 nm confocal pinhole before being sent to a photomultiplier tube to reject out of plane focused light. Every field of view (FOV) is imaged sequentially through ECFPex/ECFPem, ECFPex/EYFPem and EYFPex/EYFPem (3 excitation and emission combinations) and saved as donor, FRET and acceptor image files through an inbuilt wizard. To obtain the FRET images and efficiency of energy transfer values a RiFRET plugin in Image J software was used (Roszik et al., 2009). Prior to FRET calculations, all images were first corrected for uneven illumination, registered, and background-subtracted. Manual and automatic registration of each individual channel in ImageJ was critical to correct for motion artifacts associated with live cell imaging. Controls were performed in which images were obtained in different orders. The order in which images were obtained had no effect. FRET images were obtained by pixel-by-pixel ratiometric intensity method and efficiency of transfer was calculated by the ratio of intensity in transfer channel to the quenched (corrected) intensity in the donor channel. The following corrections were applied to all FOVs imaged: For cross-talk correction, cells transfected with CFP or YFP alone were imaged under all three previously mentioned excitation and emission combinations. FRET efficiency was quantified from 3-4 Regions of Interests (ROI) per cell drawn exclusively along the P.M. Because expression of FRET probes may have a significant impact on FRET efficiency, cells that expressed similar amounts of probes, as determined by computing the fluorescence signal/intensity by a photon counting histogram were selectively chosen for FRET analyses. Furthermore, untransfected cells and a field of view with-out cells were imaged to correct for background, autofluorescence and light scattering. To avoid artifacts of photobleaching, Oxyfluor (www.oxyrase.com) was used to minimize the formation of reactive oxygen species.

Statistical Analyses: Data presented is representative of at-least 3 independent experiments and statistical significance was assessed by student t test, where p value < 0.05 at 95% was considered statistically significant. Statistical plots, including the Gaussian kernel density plot to the histogram were generated using GraphPad or OriginLab softwares.

SUPPLEMENTARY TABLES

Table S1: PhosphositePlus®(PSP) mining for Phosphoproteins observed in cancers [Related to Figure 1]. The PhosphoSitePlus(PSP) was mined for proteins expressed in all cancers. The search yielded 535 phosphosites in 324 proteins.

See Excel File – Table S1

Table S2: PhosphositePlus®(PSP) mining for Phosphoproteins observed in cancers that are not found in normal tissues [Related to Figure 1]. The PhosphoSitePlus(PSP) was mined for proteins expressed in all cancers and also excluded if expressed in normal tissue. The search yielded 113 phosphosites in 72 proteins.

See Excel File – Table S2

Table S3: PhosphositePlus®(PSP) mining revealed phosphoproteins observed in cancers that are also involved in cellular processes [Related to Figure 1]. The PhosphoSitePlus(PSP) was mined for proteins expressed in all cancers, excluded if expressed in normal tissue, and also involved in cellular processes. Such search yielded 149 phosphosites in 92 proteins.

See Excel File – Table S3

Table S4: PhosphositePlus®(PSP) mining for Phosphoproteins observed in cancers that are also binders and/or remodelers of actin [Related to Figure 1]. The PhosphoSitePlus(PSP) was mined for proteins expressed in all cancers, excluded if expressed in normal tissue, involved in cellular processes, and involved in regulating actin. The search yielded 63 phosphosites in 42 proteins.

See Excel File – Table S4

Table S5: PhosphositePlus®(PSP) mining for Phosphoproteins observed in cancers that are actin-binding adaptors/scaffolds and are involved in cell migration [Related to Figure 1]. The PhosphoSitePlus(PSP) was mined for proteins expressed in all cancers, excluded if expressed in normal tissue, involved in cellular processes, involved in regulating actin and also involved in migration. The search yielded 34 phosphosites in 16 proteins.

See Excel File – Table S5
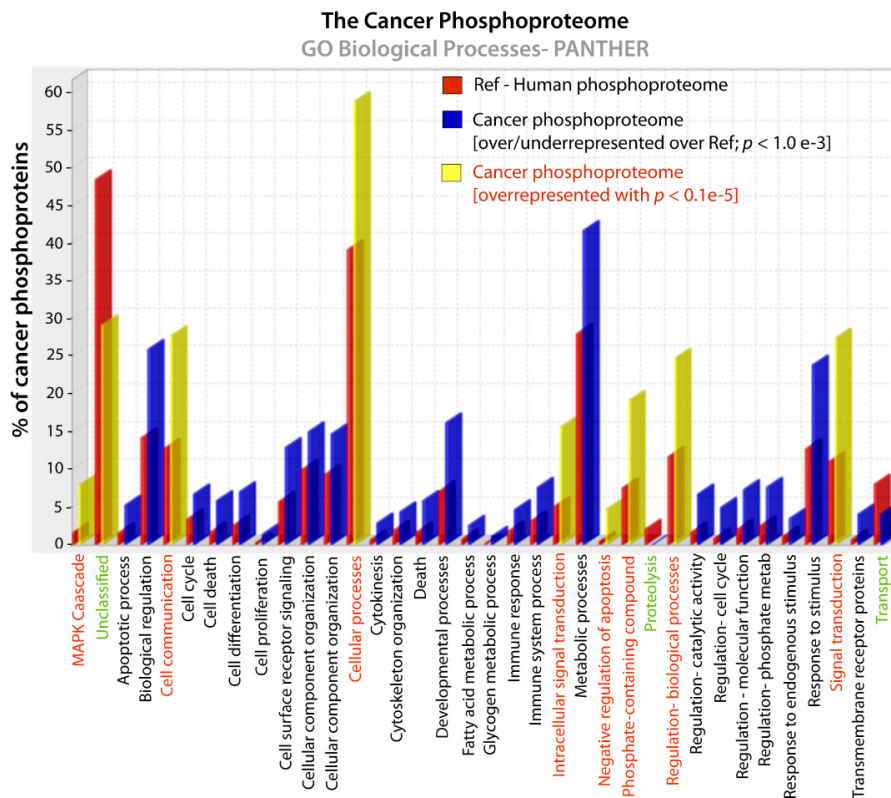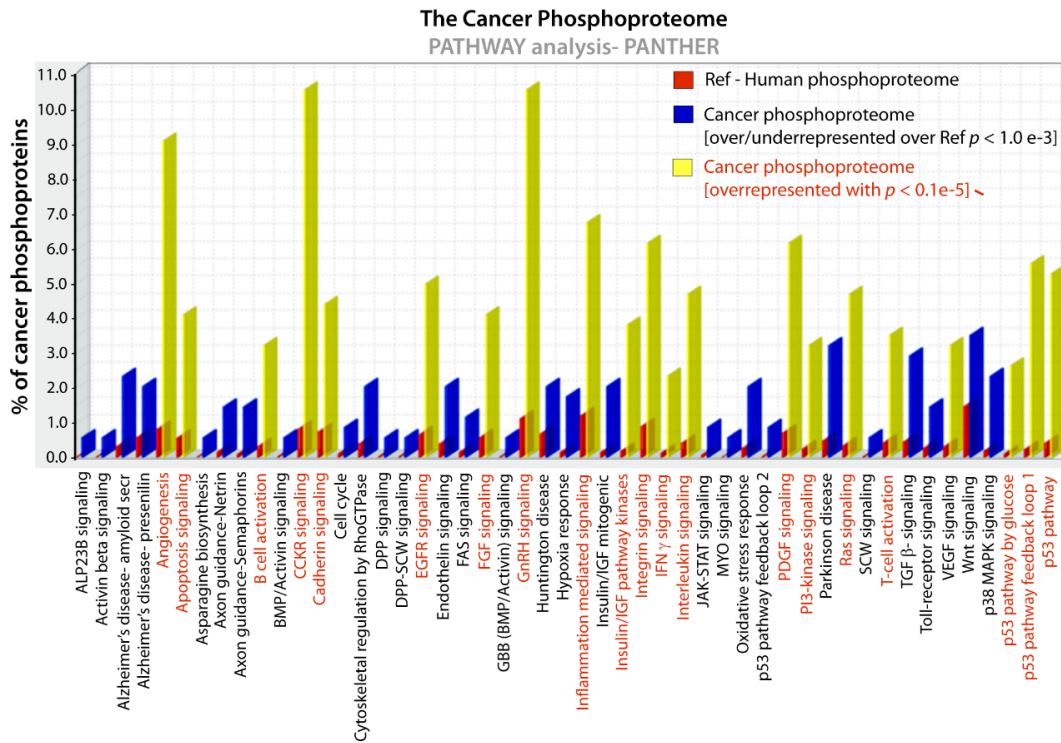
SUPPLEMENTARY FIGURES AND LEGENDS

Figure S1. Mining the PhosphositePlus® (PSP) database for pan-cancer phosphoproteome [Related to Figure 1]. A list of 324 proteins whose phosphosites are observed in cancers (see **Table S1**) were subjected to an enrichment analysis using analysis tools from the PANTHER Classification System (Mi et al., 2013). Pathways (a) and GO-biological processes (b) enriched among these 324 proteins compared to the entire human phosphoproteome as reference are displayed. % of protein in the category is calculated for each list (the human phosphoproteome reference list and the pan- cancer phosphoproteome list) as: (# proteins for the category/ # proteins in the list) X 100. Underrepresented pathways are highlighted in green.
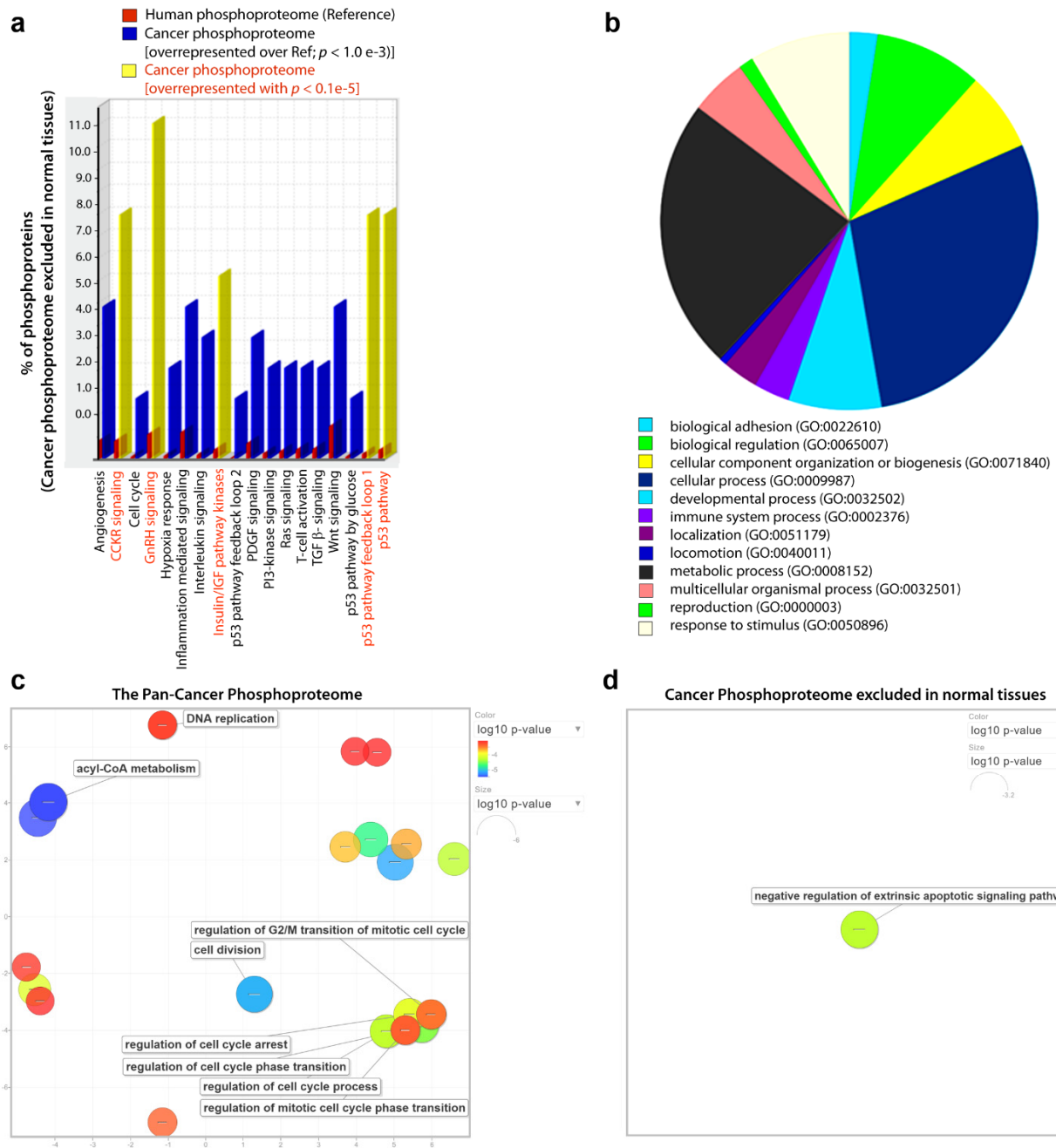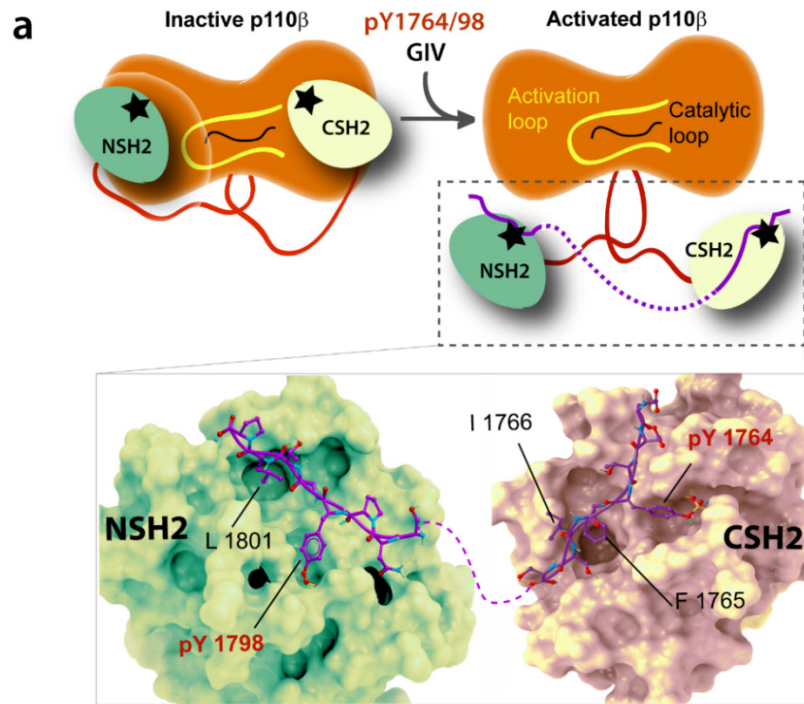
Figure S2. Mining the PhosphositePlus (PSP) database and visualizing GO enrichment in the cancer-specific phosphoproteome [Related to Figure 1]. (a-b) A list of 72 phosphoproteins from the PSP database that fit the criteria for being found in cancers but excluded in normal tissues (see **Table S2**) were subjected to an enrichment analysis using analysis tools from the PANTHER Classification System (Mi et al., 2013). Pathways (a) and GO biological processes (b) enriched among these 72 proteins compared to the entire human phosphoproteome as reference are displayed. (c-d) The list of phosphoproteins observed in cancers (**Table S1**) and the list of phosphoproteins observed in cancers but excluded in normal tissues (**Table S2**) were submitted to the Reduce + Visualize Gene Ontology (REVIGO (Supek et al., 2011)) analysis tool and GO terms were visualized in a semantic similarity-based scatterplots on left and right, respectively. GO-biological process enriched in the pan-cancer phosphoproteome (left) is notable for regulators of cell cycle, DNA replication and multiple metabolic pathways. By contrast, negative regulation of apoptotic signaling pathway is the only GO-biological process that is enriched in the cancer-specific phosphoproteome (i.e., phosphoproteins observed in cancers, not in normal tissues). The colors do not reflect pathway direction but rather the degree of statistical significance. Red circles indicate regulated pathways that are different to a highly significant degree; green and blue also indicate significant difference, but to a lesser degree. The color intensity represents the negative log10 *p* value for each of the statistically enriched pathways shown on the scatterplot.

Figure S3. **Rationale for the modular design of IMP probes [Relevant to Figure 1].** (a) Previously validated (Lin et al., 2011) structural basis for activation of PI3K by GIV is displayed. Phosphotyrosines 1764 and 1798 on GIV directly bind p85α (SH2-domains) and activate Class 1 PI3Ks. (b) Various GIV-derived IMPs generated and tested in this work; they either contain the two short stretches of sequence flanking either tyrosine 1764 or 1798 alone, or together (entire SH2 module) or in combination with GIV's GEF module (entire C-Term). Non-phosphorylatable phenylalanine mutants were generated in each case to serve as negative controls. These GIV substrates were inserted within the IMP probe shown in *Fig 1c*.
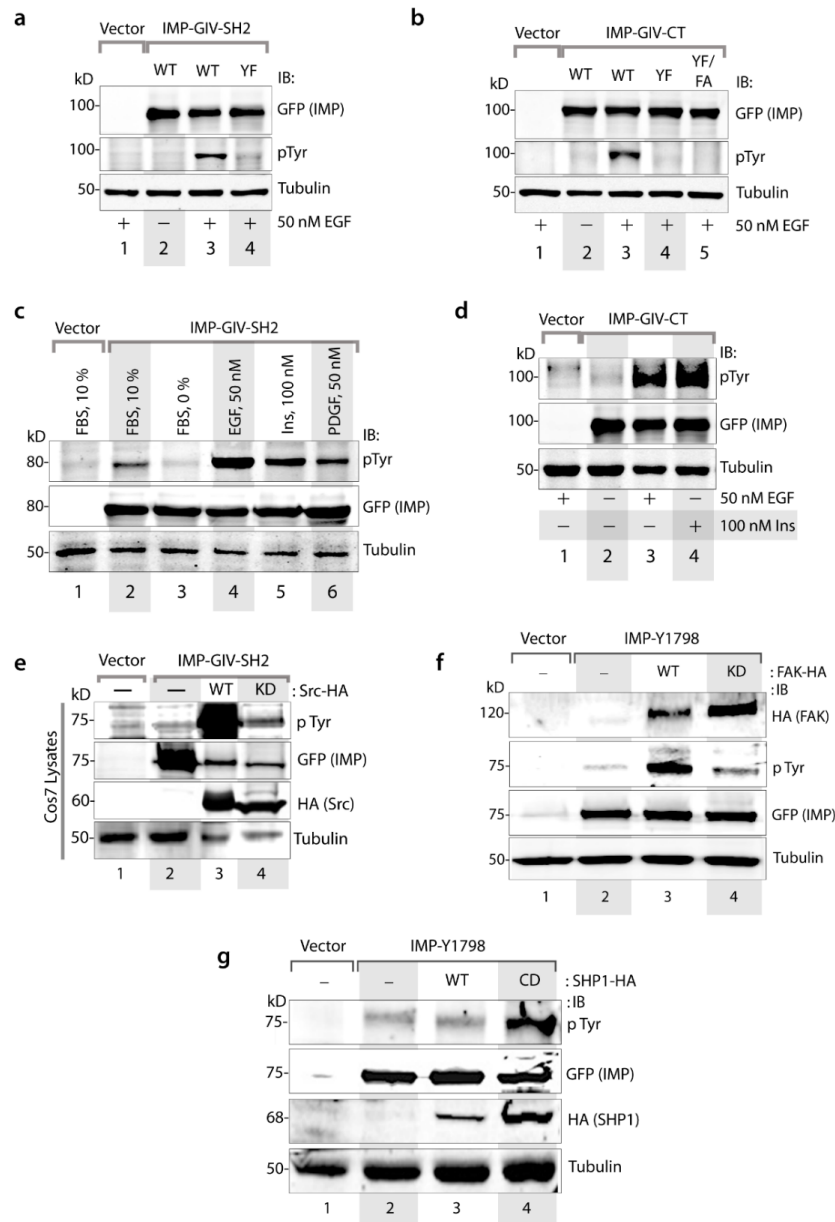
Figure S4. GIV-derived IMP probes are reversibly tyrosine phosphorylated in cells [Related to Figure 1]. (a) Immunoblots showing the phosphorylation status of WT IMP-GIV-SH2 and its corresponding YF mutant after EGF stimulation. Only WT IMP peptides are phosphorylated but not its corresponding YF mutants. (b) Immunoblots showing the phosphorylation status of WT IMP-GIV-CT and their corresponding YF and YF/FA mutants after EGF stimulation. Only WT IMP-GIV-CT probe gets phosphorylated but not its corresponding YF mutant (c) Serum-starved Cos7 cells expressing WT IMP-GIV-SH2 were stimulated with various growth factors prior to lysis. Lysates were immunoprecipitated with anti-GFP mAb and tyrosine phosphorylation of IMP-GIV-SH2 probe was analyzed by immunoblotting (IB). Phosphorylation of the peptide was observed in fed state (10% FBS) or when stimulated with EGF or Insulin or PDGF but not in overnight starved conditions. (d) Serum-starved Cos7 cells expressing WT IMP-GIV-CT were stimulated with EGF or Insulin prior to lysis. Lysates were immunoprecipitated with anti-GFP mAb and tyrosine phosphorylation of IMP was analyzed by immunoblotting (IB). Phosphorylation of the IMP-GIV-CT-WT probe was only observed in cells when stimulated with either EGF or insulin but not in starved cells. (e) Lysates of Cos7 cells co-expressing IMP-GIV-SH2 and wild-type (WT) or kinase-dead (KD) Src-HA were immunoprecipitated and analyzed for tyrosine phosphorylation of IMP as in d. Phosphorylation of the IMP-GIV-SH2 probe was only observed in cells co-transfected with Src-HA-WT but not in cells transfected with kinase dead Src-HA-KD cells. (f) Lysates of Cos7 cells expressing IMP-GIVY1798 and wild-type (WT) or Kinase Dead (KD) FAK-HA were immunoprecipitated and analyzed for tyrosine phosphorylation of IMP as in d. Phosphorylation of the IMP-GIV-SH2 probe was only detected in cells expressing WT-FAK-HA but in kinase dead FAK-HA expressing cells. (g) Lysates of Cos7 cells expressing IMP-GIV&1798 and wild-type (WT) or catalytically dead (CD) SHP1-HA were immunoprecipitated and analyzed for tyrosine phosphorylation of IMP as in d. Phosphorylation of the IMP-GIVY1798 probe was only detected in cells expressing SHP1-HA-CD but in SHP1-HA-WT expressing cells.
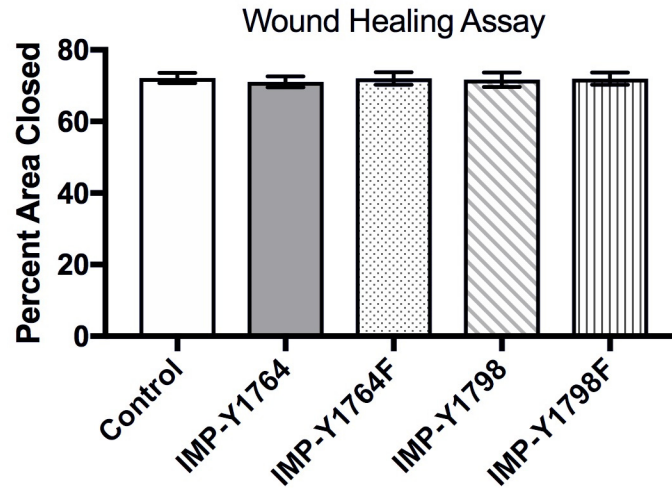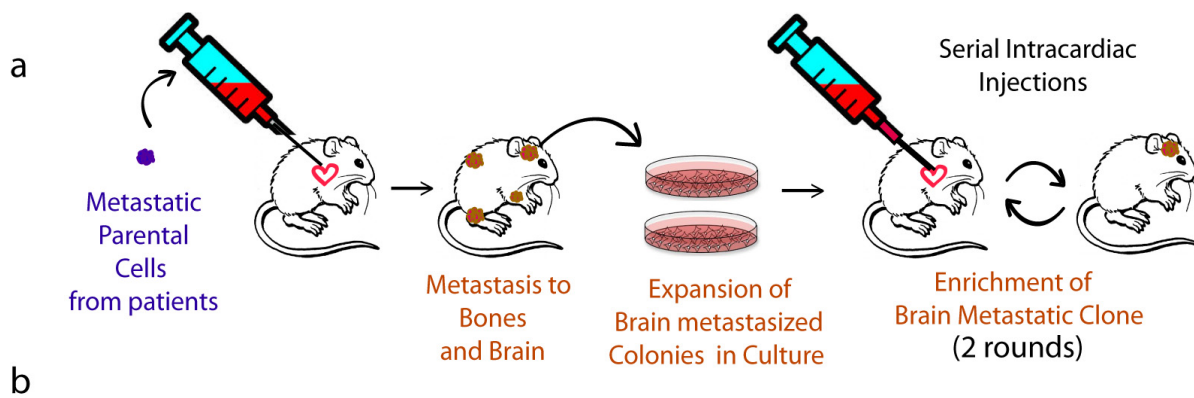
Figure S5. Transient overexpression of IMP 1764 and IMP1798 does not alter 2D cell migration in scratch-wound assays [Related to Figure 1]. Sub-confluent (~85-90%) monolayers of HeLa cells transiently transfected with the indicated IMP constructs were grown to confluence over 30 h prior to scratch-wounding. Wounds were imaged immediately after wounding and again, after 12 and 24 hours by light microscopy. Bar graphs display the % wound closure, as determined by tracing the exposed wound area at the beginning and at 24 h using ImageJ was measured. Error bars represent ±SEM; n = 4-5 wounds per cell line, per experiment, from 3 independent biological repeat experiments.

Paired Cell Lines	Type of Cancer	Source of Parental Cells	Known Genetic Mutations	Ref PMID (Source Lab)
MDAMB231 (Parental and Brain Metastatic Clone)	Human Breast Adenocarcinoma	Metastatic Pleural Effusion	*KRAS* G13D, *BRAF* G464V PMID: 17314276	24581498 (J. Massague)
PC-9 (Parental and Brain Metastatic Clone)	Human Lung Adenocarcinoma	Metastatic clone from lymph node	KRAS (G12C) PMID: 8806092	19576624 24581498 (J. Massague)
H2030 (Parental and Brain Metastatic Clone)	Human Lung Adenocarcinoma	Metastatic clone from lymph node	*EGFR*$^{\Delta exon19}$ PMID: 15761868, PMID: 1847845	19576624 24581498 (J. Massague)
21T (16N, NT, MT2)	Human Breast Infiltrating and intraductal mammary carcinoma (ER-/PR-; Node +) PMID: 1977518	16N = Normal, Contralateral Breast NT = Primary Tumor MT2 = Metastatic Pleural Effusion	In NT and MT2 - p53 (frameshift mutation, loss of function (PMID: 7923592)	20198662 20458274 17545609 (A. Pardee)

Figure S6. Sources of various paired cancer cell lines used in the study [Related to Figure 3]. (a) Schematic representing the technique that was employed by Massague et al (Nguyen et al., 2009) to generate paired primary and Brain metastatic clones. Briefly, 10^5 of metastatic lung or breast cancer cells isolated from lymphatic duct or pleural effusions of cancer patients were injected into arterial circulation of nude mice. Subsequently, tumor cells were isolated from lesions formed at secondary site i. e. brain or bone, followed by expansion of the cells and reinjection of the cells into mice circulation for two more rounds to select for highly metastatic clones. (b) List of paired (parental and brain mets) lung and breast cancer cell lines with variable metastatic proclivity used in the study, their varying genetic background, and known mutations and the sources of cells.
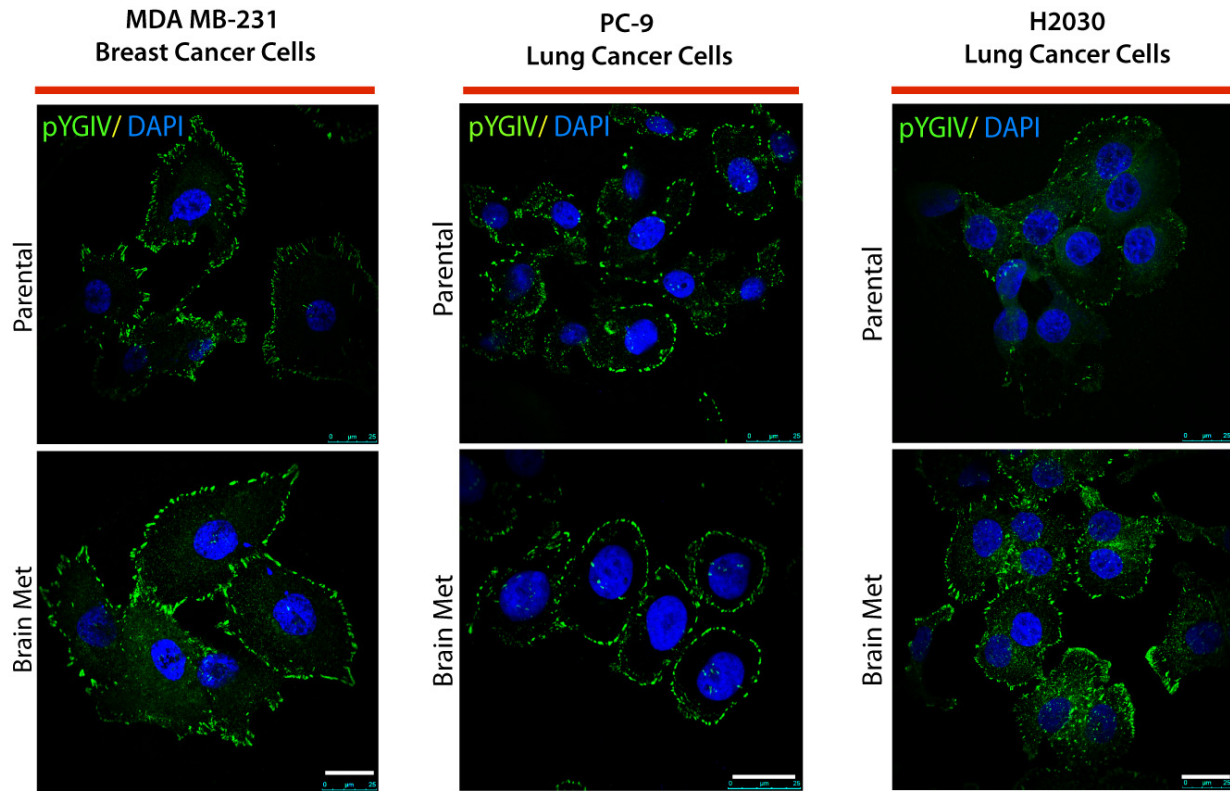
Figure S7. Tyrosine phosphorylation of GIV is indistinguishable among paired primary and BrM breast and lung cancer cells by Immunofluorescence [Related to Figure 3]. PC-9, H2030, MDA-MB-231 primary and their BrM counterparts were fixed, stained for tyrosine phosphorylated GIV (pYGIV; red) and DAPI (nucleus; blue) and analyzed by confocal microscopy. Representative images of cells are shown. Although cell-to-cell heterogeneity in intensity of staining was encountered, no discernable differences in patterns of staining was observed between the parental and BrM clones. Bar = 10 μm.
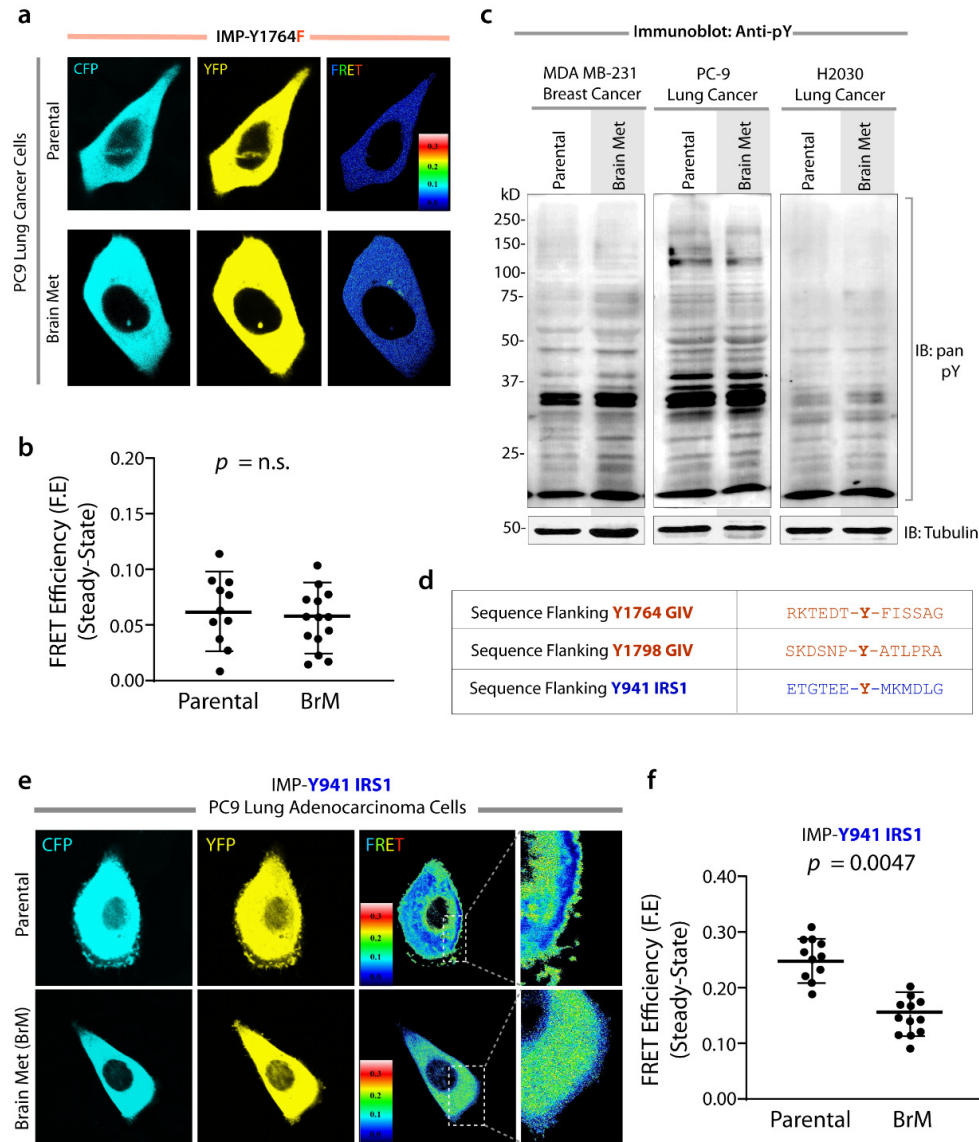
Figure S8. Control experiments that show the specificity of IMP probes to detect meaningful, context-dependent signals [Related to Figure 3]. (a-b) Representative steady state FRET images of PC-9 parental and BrM cells expressing IMP-Y1764F mutant probe. IMP Y1764F mutant peptide shows no differential FRET signal when expressed in paired cancer cell lines; very little FRET was observed in both the parental and BrM PC-9 cell groups at steady state in 10% serum, indicating that tyrosine phosphorylation of the IMP probe is essential for the differential FRET observed in these cells using the WT probe *2e*. (b) Scatter plots display the FRET efficiency at the PM in *a*. Results are expressed as mean ± S.D. (c) Whole cell lysates from paired PC-9, H2030 and MDA-MB-231 cells were immunoblotted with total phosphorylated tyrosine antibody. Full-length phosphotyrosine immunoblot shows no discernable differences in either global tyrosine phosphorylation or tyrosine phosphorylation at any given molecular weight between the parental and the BrM clones. Results indicate that the differences in FRET in these paired cells observed using the IMP-Y1764 probe in *2d-f* does not merely reflect global differences in tyrosine phosphorylation. (d-f) Replacement of the GIV substrate sequence with a sequence derived from IRS1 abolishes the ability of IMP probes to distinguish cancer cells with high from low metastatic potential. (d) Schematic showing the substrate sequence of GIV used in IMP-Y1764 and IMP-Y1798 probes, and the sequence of IRS1 that was used to substitute the residues flanking the Y substrate. Previous work has shown that this site is phosphorylated by multiple growth factors (EGF, PDGF and Insulin) (Sato et al., 2002) and is a binding site for p85α(PI3K) (Yonezawa et al., 1992) and induces FRET when used in similar probe design as IMPs (Sato et al., 2002). (e) Parental and brain metastatic (BrM) clones of PC-9 lung cancer cells expressing IMP-Y941 IRS were analyzed for steady-state FRET by confocal live-cell imaging. Representative CFP, YFP and FRET images are shown. Boxed area on the left is magnified on the right. FRET is frequently observed at the PM in parental, but not in BrM clones. (f) Scatter plots display the FRET efficiency at the PM in e. Results are expressed as mean ± S.D.
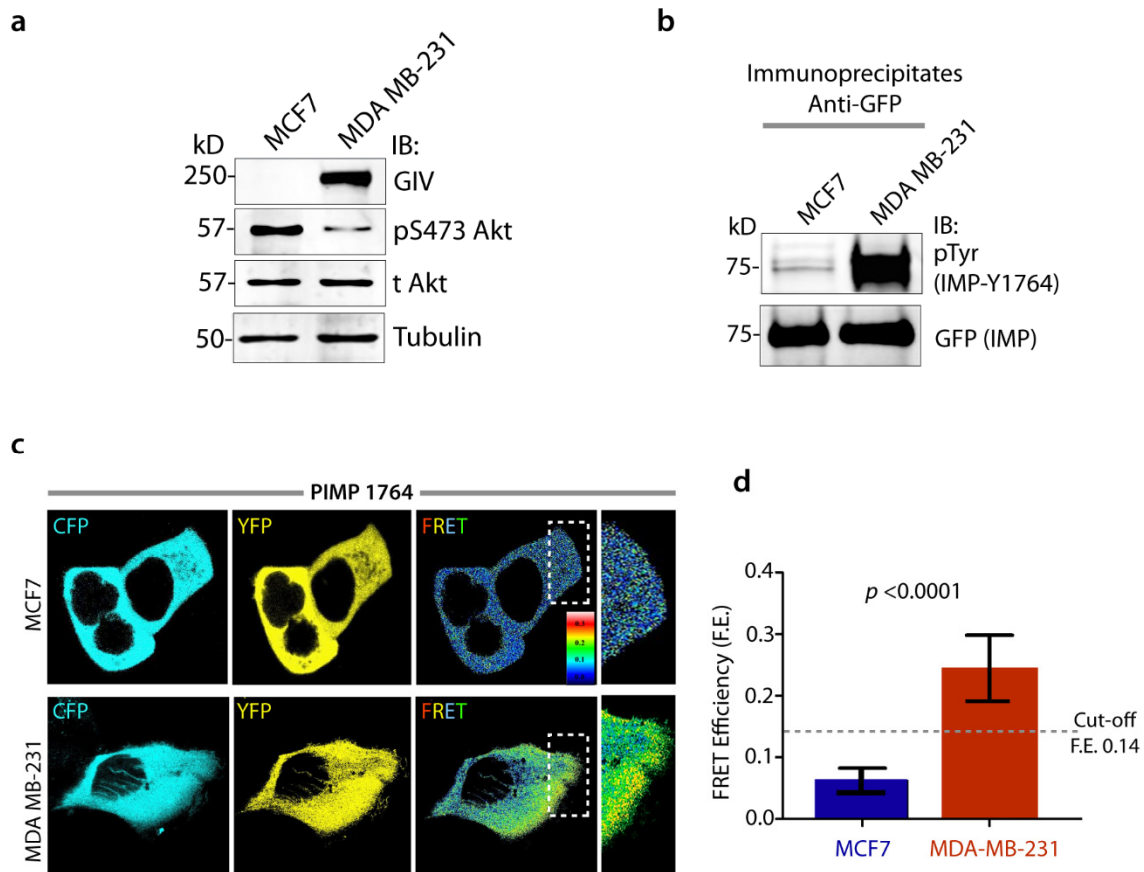
Figure S9. IMP sensors can distinguish between MCF7 and MDA-MB-231 cells, two breast cancer cell lines with contrasting metastatic proclivities [Related to Figure 3]. (a) Whole cell lysates of MCF7 and MDA-MB-231 cells were analyzed for GIV, phospho(p)Akt, total(t)Akt and tubulin by immunoblotting (IB). (b) Immunoprecipitation was carried out from lysates of MCF7 and MDA-MB-231 cells expressing IMP-Y1764 with anti-GFP mAb and analyzed for tyrosine phosphorylation of IMP by immunoblotting (IB). (c) MCF7 and MDA-MB-231 cells expressing IMP-Y1764 were analyzed for steady-state FRET by confocal live-cell imaging. Representative CFP, YFP and FRET images are shown. Boxed area on the left is magnified on the right. (d) Bar graphs display the FRET efficiency (F.E) in c. The cut-off F.E of 0.14 (based on the cumulative histograms in *Fig 3g*) denotes that MCF7 cells with low F.E and MDA-MB-231 cells with high F.E have low and high metastatic potentials, respectively. Results are expressed as mean ± S.D.
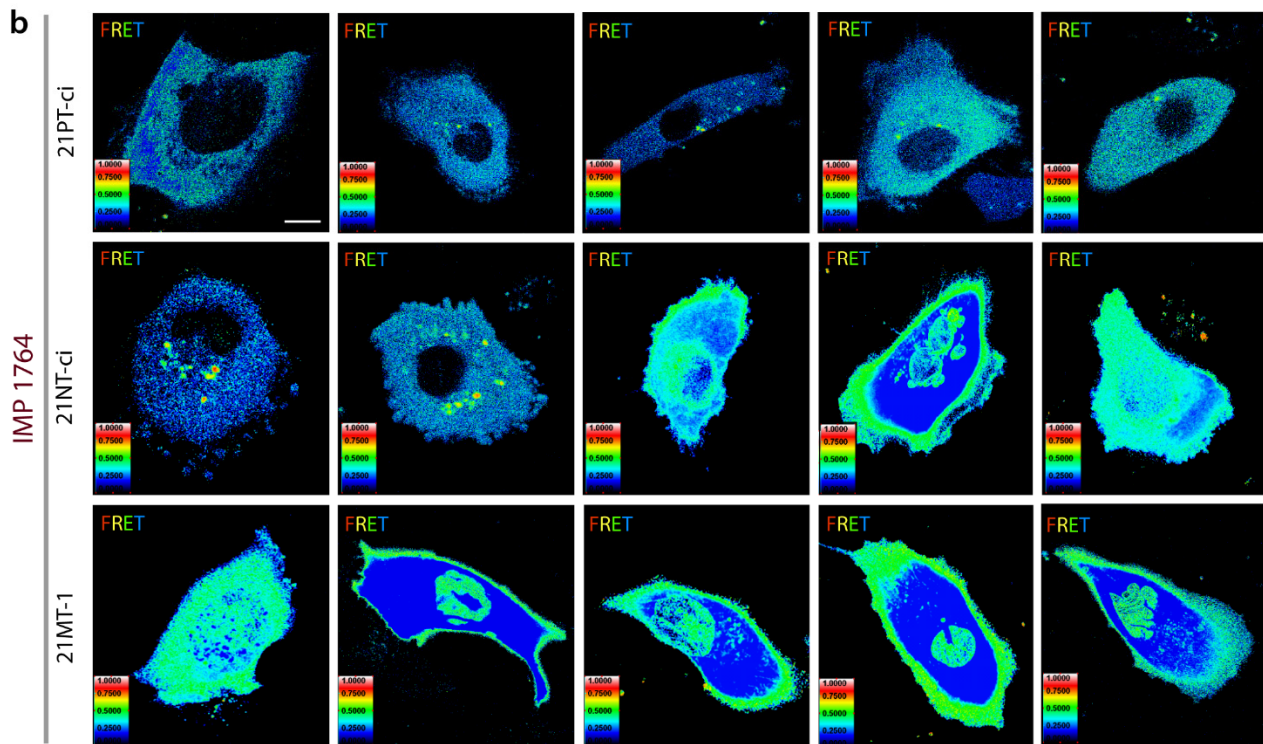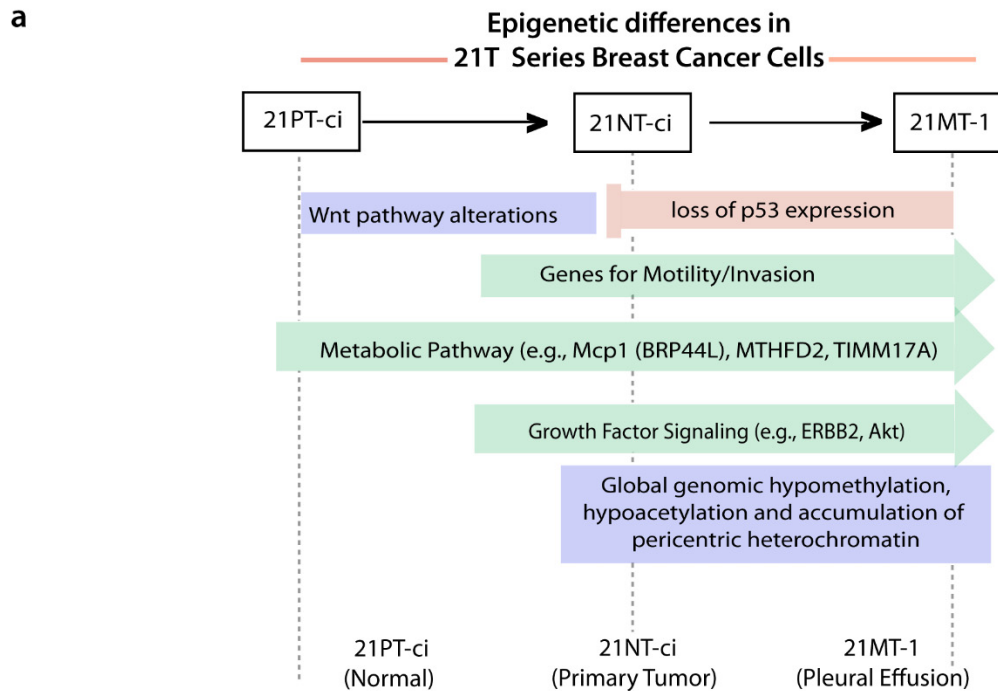
Figure S10. IMPY1764 sensor retains its ability to detect metastatic proclivity despite the evolving genetic and epigenetic shifts in tumor cells during the course of metastatic progression [Related to Figure 3]. (a) Schematic summarizing the characteristics of the 21T series of breast cancer cells. These isogenic cells were derived from the same patient (#21) during breast cancer progression (Band et al., 1990) (*Fig 3h*). The array of evolving epigenetic (Liu et al., 1994; Santos et al., 2014; Souter et al., 2010), proteomic (Xu et al., 2010) and signaling (MacMillan et al., 2014; Qiao et al., 2007) programs during progressive acquisition of metastatic potential are summarized. *(b)* 21T cells expressing IMP-Y1764 were analyzed for steady-state FRET by confocal live-cell imaging. Representative FRET images are shown as a montage of single-cells images. Quantifications are displayed as scatter plots in *Fig 3i*.
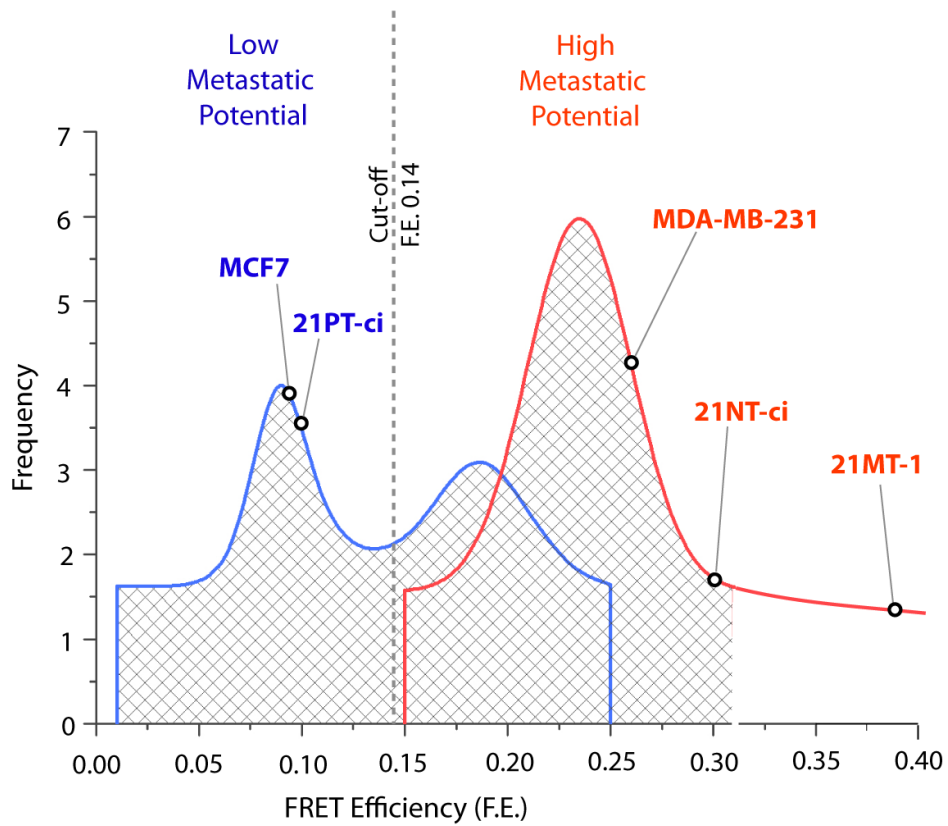
Figure S11. Gaussian Fits of FRET histograms [Related to Figure 3]. Gaussian fits of the cumulative histogram in *Fig 3g* is displayed here with the position of various cell lines (mean FRET) studied in this work indicated on the gaussian curve.

a

| Paired Cell Lines	Type of Cancer	Pathways Upregulated During Drug Resistance	Known Genetic Abnormalities	Ref PMID (Source Lab)
Hs578T (Docetaxel sensitive vs resistant)	Human Breast	Multiple pathways, including mTOR and TNF-dependent NF-κB survival pathways. (PMID: 15718313; 12907009)	ER -ve; Hypotriploid human cell line with a modal chromosome number of 59 (ATCC.org) (PMID: 864756)	ATCC
HCC827 (Erlotinib sensitive vs resistant)	Human Lung Adenocarcinoma	PI3K (PMID: 21220474) Non-RTK Signaling (Src/FAK) (PMID:25193862; 19804422) Gowth Factor RTK Signaling (cMet, VEGF, IGFR) (PMID:24828661; 22133747; 21062933; 19921194; 19447865) STAT3 (PMID: 23894143) mTOR (PMID: 23690929)	EGFR tyrosine kinase domain (E746 - A750 deletion) (ATCC.org)	Frank Furnari (UCSD)
HCC827 (Lapatinib sensitive vs resistant)	Human Lung Adenocarcinoma	--	EGFR tyrosine kinase domain (E746 - A750 deletion) (ATCC.org)	David Cheresh (PMID: 24747441)
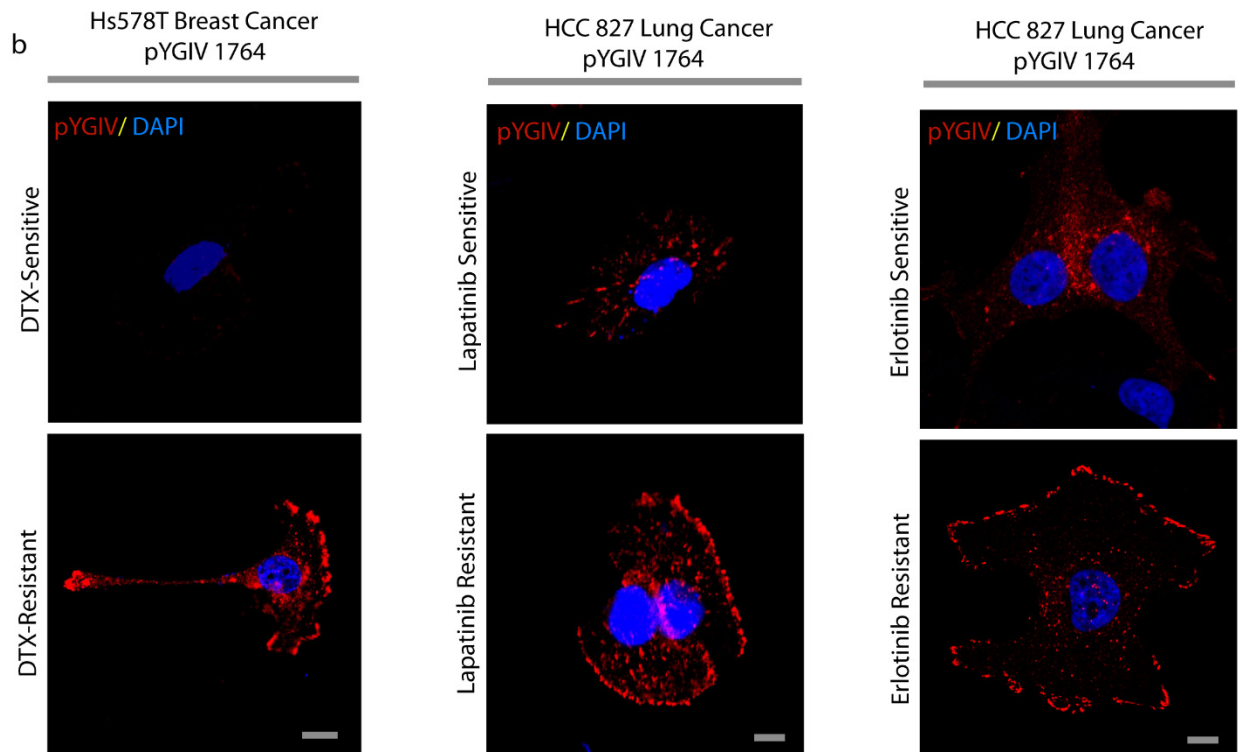
Figure S12. Tyrosine phosphorylation of GIV at the PM is enhanced during drug resistance [Related to Figure 4]. (a) Table lists the paired (sensitive vs resistant) breast (Hs578T) and lung (HCC827) cancer cells used in this study, the underlying pathways implicated in the development of drug resistance, the genetic background and the source of cells. (b) Docetaxel (DTX)-sensitive and resistant pairs of Hs578T, and Lapatinib/Erlotinib sensitive and resistant pairs of HCC827 cells were fixed, stained for tyrosine phosphorylated GIV (pYGIV; red) and DAPI (nucleus; blue) and analyzed by confocal microscopy. Representative images of cells are shown. Bar = 10 μm.

SUPPLEMENTARY MOVIE CAPTIONS

SM1. Dynamic changes in FRET at the PM upon EGF stimulation of Cos7 cells expressing the IMP-pY1764 probe [Related to Figure 2]. Movie shows ligand-dependent signaling via the GIV-PI3K axis as visualized through FRET imaging in living Cos7 cells expressing the wild type IMP-Y1764 sensor.

SM2. Loss of dynamic changes in FRET upon EGF stimulation [Related to Figure 2]. Movie shows loss of FRET upon EGF stim in of Cos7 cells expressing the non-phosphorylatable IMP-pY1764F mutant probe, indicating that phosphorylation and phosphorylation-induced intramolecular rearrangement of the probe is required for the observed changes in FRET in SM1.

SM3. Dynamic changes in FRET at the PM upon EGF stimulation of Cos7 cells expressing the IMP-pY1798 probe [Related to Figure 2]. Movie shows ligand-dependent signaling via the GIV-PI3K axis as visualized through FRET imaging in living Cos7 cells expressing the wild type IMP-Y1798 sensor.

SM4. Loss of dynamic changes in FRET upon EGF stimulation of Cos7 cells expressing the non-phosphorylatable IMP-pY1798F mutant probe [Related to Figure 2]. This movie indicates that phosphorylation and phosphorylation-induced intramolecular rearrangement of the probe is required for the observed changes in FRET in SM3.

SM5. Dynamic changes in FRET at the PM upon LPA stimulation of Cos7 cells expressing the IMP-pY1764 probe [Related to Figure 2]. Movie shows ligand-dependent signaling via the GIV-PI3K axis as visualized through FRET imaging in living Cos7 cells expressing the wild type IMP-Y1764 sensor.

SM6. Loss of dynamic changes in FRET upon LPA stimulation of Cos7 cells expressing the non-phosphorylatable IMP-pY1764F mutant probe [Related to Figure 2]. This movie indicates that phosphorylation and phosphorylation-induced intramolecular rearrangement of the probe is required for the observed dynamic changes in FRET in SM5.

SUPPLEMENTARY BIBLIOGRAPHY

Band, V., Zajchowski, D., Swisshelm, K., Trask, D., Kulesa, V., Cohen, C., Connolly, J., and Sager, R. (1990). Tumor progression in four mammary epithelial cell lines derived from the same patient. Cancer research *50*, 7351-7357.

Borejdo, J., Rich, R., and Midde, K. (2012). Mesoscopic analysis of motion and conformation of cross-bridges. Biophys Rev *4*, 299-311.

Broussard, J.A., Rappaz, B., Webb, D.J., and Brown, C.M. (2013). Fluorescence resonance energy transfer microscopy as demonstrated by measuring the activation of the serine/threonine kinase Akt. Nature protocols *8*, 265-281.

Brown, I., Shalli, K., McDonald, S.L., Moir, S.E., Hutcheon, A.W., Heys, S.D., and Schofield, A.C. (2004). Reduced expression of p27 is a novel mechanism of docetaxel resistance in breast cancer cells. Breast cancer research : BCR *6*, R601-607.

Garcia-Marcos, M., Ghosh, P., and Farquhar, M.G. (2009). GIV is a nonreceptor GEF for G alpha i with a unique motif that regulates Akt signaling. Proceedings of the National Academy of Sciences of the United States of America *106*, 3178-3183.

Garcia-Marcos, M., Jung, B.H., Ear, J., Cabrera, B., Carethers, J.M., and Ghosh, P. (2011). Expression of GIV/Girdin, a metastasis-related protein, predicts patient survival in colon cancer. FASEB journal : official publication of the Federation of American Societies for Experimental Biology *25*, 590-599.

Ghosh, P., Beas, A.O., Bornheimer, S.J., Garcia-Marcos, M., Forry, E.P., Johannson, C., Ear, J., Jung, B.H., Cabrera, B., Carethers, J.M.*, et al.* (2010). A Gi-GIV Molecular Complex Binds Epidermal Growth Factor Receptor and Determines whether Cells Migrate or Proliferate. Molecular biology of the cell.

Griesbeck, O., Baird, G.S., Campbell, R.E., Zacharias, D.A., and Tsien, R.Y. (2001). Reducing the environmental sensitivity of yellow fluorescent protein. Mechanism and applications. The Journal of biological chemistry *276*, 29188-29194.

Jost, C.A., Reither, G., Hoffmann, C., and Schultz, C. (2008). Contribution of fluorophores to protein kinase C FRET probe performance. Chembiochem *9*, 1379-1384.

Kotera, I., Iwasaki, T., Imamura, H., Noji, H., and Nagai, T. (2010). Reversible dimerization of Aequorea victoria fluorescent proteins increases the dynamic range of FRET-based indicators. ACS Chem Biol *5*, 215-222.

Lane, J.R., Powney, B., Wise, A., Rees, S., and Milligan, G. (2008). G protein coupling and ligand selectivity of the D2L and D3 dopamine receptors. The Journal of pharmacology and experimental therapeutics *325*, 319-330.

Li, C., Wen, A., Shen, B., Lu, J., Huang, Y., and Chang, Y. (2011). FastCloning: a highly simplified, purification-free, sequence- and ligation-independent PCR cloning method. BMC biotechnology *11*, 92.

Lin, C., Ear, J., Pavlova, Y., Mittal, Y., Kufareva, I., Ghassemian, M., Abagyan, R., Garcia-Marcos, M., and Ghosh, P. (2011). Tyrosine phosphorylation of the Galpha-interacting protein GIV promotes activation of phosphoinositide 3-kinase during cell migration. Science signaling *4*, ra64.

Liu, X.L., Band, H., Gao, Q., Wazer, D.E., Chu, Q., and Band, V. (1994). Tumor cell-specific loss of p53 protein in a unique in vitro model of human breast tumor progression. Carcinogenesis *15*, 1969-1973.

Lopez-Sanchez, I., Dunkel, Y., Roh, Y.S., Mittal, Y., De Minicis, S., Muranyi, A., Singh, S., Shanmugam, K., Aroonsakool, N., Murray, F.*, et al.* (2014). GIV/Girdin is a central hub for profibrogenic signalling networks during liver fibrosis. Nature communications *5*, 4451.

MacMillan, C.D., Leong, H.S., Dales, D.W., Robertson, A.E., Lewis, J.D., Chambers, A.F., and Tuck, A.B. (2014). Stage of breast cancer progression influences cellular response to activation of the WNT/planar cell polarity pathway. Scientific reports *4*, 6315.

Mi, H., Muruganujan, A., Casagrande, J.T., and Thomas, P.D. (2013). Large-scale gene function analysis with the PANTHER classification system. Nature protocols *8*, 1551-1566.

Midde, K., Rich, R., Saxena, A., Gryczynski, I., Borejdo, J., and Das, H.K. (2014). Membrane topology of human presenilin-1 in SK-N-SH cells determined by fluorescence correlation spectroscopy and fluorescent energy transfer. Cell biochemistry and biophysics *70*, 923-932.

Midde, K.K., Aznar, N., Laederich, M.B., Ma, G.S., Kunkel, M.T., Newton, A.C., and Ghosh, P. (2015). Multimodular biosensors reveal a novel platform for activation of G proteins by growth factor receptors. Proceedings of the National Academy of Sciences of the United States of America *112*, E937-946.

Mittal, Y., Pavlova, Y., Garcia-Marcos, M., and Ghosh, P. (2011). Src homology domain 2-containing protein-tyrosine phosphatase-1 (SHP-1) binds and dephosphorylates G(alpha)-interacting, vesicle-associated protein (GIV)/Girdin and attenuates the GIV-phosphatidylinositol 3-kinase (PI3K)-Akt signaling pathway. The Journal of biological chemistry *286*, 32404-32415.

Nguyen, D.X., Chiang, A.C., Zhang, X.H., Kim, J.Y., Kris, M.G., Ladanyi, M., Gerald, W.L., and Massague, J. (2009). WNT/TCF signaling through LEF1 and HOXB9 mediates lung adenocarcinoma metastasis. Cell *138*, 51-62.

Qiao, M., Iglehart, J.D., and Pardee, A.B. (2007). Metastatic potential of 21T human breast cancer cells depends on Akt/protein kinase B activation. Cancer research *67*, 5293-5299.

Roszik, J., Lisboa, D., Szollosi, J., and Vereb, G. (2009). Evaluation of intensity-based ratiometric FRET in image cytometry--approaches and a software solution. Cytometry Part A : the journal of the International Society for Analytical Cytology *75*, 761-767.

Santos, G.C., Jr., da Silva, A.P., Feldman, L., Ventura, G.M., Vassetzky, Y., and de Moura Gallo, C.V. (2014). Epigenetic modifications, chromatin distribution and TP53 transcription in a model of breast cancer progression. Journal of cellular biochemistry.

Sato, M., Ozawa, T., Inukai, K., Asano, T., and Umezawa, Y. (2002). Fluorescent indicators for imaging protein phosphorylation in single living cells. Nature biotechnology *20*, 287-294.

Souter, L.H., Andrews, J.D., Zhang, G., Cook, A.C., Postenka, C.O., Al-Katib, W., Leong, H.S., Rodenhiser, D.I., Chambers, A.F., and Tuck, A.B. (2010). Human 21T breast epithelial cell lines mimic breast cancer progression in vivo and in vitro and show stage-specific gene expression patterns. Laboratory investigation; a journal of technical methods and pathology *90*, 1247-1258.

Supek, F., Bosnjak, M., Skunca, N., and Smuc, T. (2011). REVIGO summarizes and visualizes long lists of gene ontology terms. PLoS One *6*, e21800.

Ullman, K.S., Powers, M.A., and Forbes, D.J. (1997). Nuclear export receptors: from importin to exportin. Cell *90*, 967-970.

Valiente, M., Obenauf, A.C., Jin, X., Chen, Q., Zhang, X.H., Lee, D.J., Chaft, J.E., Kris, M.G., Huse, J.T., Brogi, E.*, et al.* (2014). Serpins promote cancer cell survival and vascular co-option in brain metastasis. Cell *156*, 1002-1016.

Xu, X., Qiao, M., Zhang, Y., Jiang, Y., Wei, P., Yao, J., Gu, B., Wang, Y., Lu, J., Wang, Z.*, et al.* (2010). Quantitative proteomics study of breast cancer cell lines isolated from a single patient: discovery of TIMM17A as a marker for breast cancer. Proteomics *10*, 1374-1390.

Yonezawa, K., Ueda, H., Hara, K., Nishida, K., Ando, A., Chavanieu, A., Matsuba, H., Shii, K., Yokono, K., Fukui, Y.*, et al.* (1992). Insulin-dependent formation of a complex containing an 85-kDa subunit of phosphatidylinositol 3-kinase and tyrosine-phosphorylated insulin receptor substrate 1. The Journal of biological chemistry *267*, 25958-25965.